27
6-16-82
I.3804 (1)
5/25

SANDIA REPORT SAND82-0481 • Unlimited Release • UC-85
Printed April 1982

Uniaxial Compression Test Series on Bullfrog Tuff

L59
10

MASTER

DO NOT MICROFILM
COVER

Ronald H. Price, Adrian K. Jones, Karol G. Nimick

Prepared by
Sandia National Laboratories
Albuquerque, New Mexico 87185 and Livermore, California 94550
for the United States Department of Energy
under Contract DE-AC04-76DP00789

DISTRIBUTION OF THIS DOCUMENT IS UNLIMITED

DISCLAIMER

This report was prepared as an account of work sponsored by an agency of the United States Government. Neither the United States Government nor any agency Thereof, nor any of their employees, makes any warranty, express or implied, or assumes any legal liability or responsibility for the accuracy, completeness, or usefulness of any information, apparatus, product, or process disclosed, or represents that its use would not infringe privately owned rights. Reference herein to any specific commercial product, process, or service by trade name, trademark, manufacturer, or otherwise does not necessarily constitute or imply its endorsement, recommendation, or favoring by the United States Government or any agency thereof. The views and opinions of authors expressed herein do not necessarily state or reflect those of the United States Government or any agency thereof.

DISCLAIMER

Portions of this document may be illegible in electronic image products. Images are produced from the best available original document.

Issued by Sandia National Laboratories, operated for the United States Department of Energy by Sandia Corporation.
NOTICE: This report was prepared as an account of work sponsored by an agency of the United States Government. Neither the United States Government nor any agency thereof, nor any of their employees, nor any of their contractors, subcontractors, or their employees, makes any warranty, express or implied, or assumes any legal liability or responsibility for the accuracy, completeness, or usefulness of any information, apparatus, product, or process disclosed, or represents that its use would not infringe privately owned rights. Reference herein to any specific commercial product, process, or service by trade name, trademark, manufacturer, or otherwise, does not necessarily constitute or imply its endorsement, recommendation, or favoring by the United States Government, any agency thereof or any of their contractors or subcontractors. The views and opinions expressed herein do not necessarily state or reflect those of the United States Government, any agency thereof or any of their contractors or subcontractors.

Printed in the United States of America
Available from
National Technical Information Service
U.S. Department of Commerce
5285 Port Royal Road
Springfield, VA 22161

NTIS price codes
Printed copy: A03
Microfiche copy: A01

DISCLAIMER

This book was prepared as an account of work sponsored by an agency of the United States Government. Neither the United States Government nor any agency thereof, nor any of their employees, makes any warranty, express or implied, or assumes any legal liability or responsibility for the accuracy, completeness, or usefulness of any information, apparatus, product, or process disclosed, or represents that its use would not infringe privately owned rights. Reference herein to any specific commercial product, process, or service by trade name, trademark, manufacturer, or otherwise, does not necessarily constitute or imply its endorsement, recommendation, or favoring by the United States Government or any agency thereof. The views and opinions of authors expressed herein do not necessarily state or reflect those of the United States Government or any agency thereof.

SAND82-0481
Unlimited Release

UNIAXIAL COMPRESSION TEST SERIES ON BULLFROG TUFF*

Ronald H. Price, Adrian K. Jones, Karol G. Nimick
Sandia National Laboratories**
Albuquerque, New Mexico 87185

SAND--82-0481

DE82 015665

ABSTRACT

Nineteen uniaxial compressive experiments were performed on samples of the Bullfrog Member of the Crater Flat Tuff, obtained from drillhole USW-G1 at Yucca Mountain on the Nevada Test Site. The water saturated samples were deformed at a nominal strain rate of 10^{-5} sec^{-1}, atmospheric pressure and room temperature. Resultant unconfined compressive strengths, axial strains to failure, Young's moduli and Poisson's ratios ranged from 4.63 to 153. MPa, .0028 to .0058, 2.03 to 28.9 GPa and .08 to .16, respectively.

* This work was supported by the U. S. Department of Energy (DOE) under Contract DE-AC04-76-DP00789.

** A U. S. DOE Facility.

DISTRIBUTION OF THIS DOCUMENT IS UNLIMITED

DISCLAIMER

This report was prepared as an account of work sponsored by an agency of the United States Government. Neither the United States Government nor any agency thereof, nor any of their employees, make any warranty, express or implied, or assumes any legal liability or responsibility for the accuracy, completeness, or usefulness of any information, apparatus, product, or process disclosed, or represents that its use would not infringe privately owned rights. Reference herein to any specific commercial product, process, or service by trade name, trademark, manufacturer, or otherwise does not necessarily constitute or imply its endorsement, recommendation, or favoring by the United States Government or any agency thereof. The views and opinions of authors expressed herein do not necessarily state or reflect those of the United States Government or any agency thereof.

DISCLAIMER

Portions of this document may be illegible in electronic image products. Images are produced from the best available original document.

TABLE OF CONTENTS

LIST OF SYMBOLS AND CONVENTIONS

σ_1, σ_2, σ_3	Principal stresses (force/original area); compressive stresses are positive
ε_1, ε_2, ε_3	Principal strains (change in length/original length); compressive strains are positive
σ_{AX}, ε_{AX}	Stress and strain parallel to cylinder cylinder axis (i.e., $\sigma_{AX} = \sigma_1$ and $\varepsilon_{AX} = \varepsilon_1$)
ε_{LAT}	Strain perpendicular to cylinder axis (i.e., lateral strain ($= \varepsilon_2 = \varepsilon_3$))
$(\sigma_{AX})_u$	Ultimate axial stress
$(\varepsilon_{AX})_u$	Axial strain corresponding to ultimate axial stress
E, ν	Elastic moduli (Young's modulus, Poisson's ratio)
F	Force
d	Displacement
T	Temperature
P	Pressure
t	Time
ϕ	Porosity
ρ_g	Grain Density

LIST OF TABLES

LIST OF FIGURES

UNIAXIAL COMPRESSION TEST SERIES ON BULLFROG TUFF

Ronald H. Price, Adrian K. Jones, Karol G. Nimick
Sandia National Laboratories
Albuquerque, New Mexico 87185

INTRODUCTION

Yucca Mountain, near the SW margin of the Nevada Test Site (NTS) in southern Nevada, is being evaluated as a potential site for underground storage of nuclear wastes. Yucca Mountain primarily consists of layered volcanic tuff (Lipman and McKay, 1965). At present, four stratigraphic units are being tested for physical, thermal and mechanical properties as part of the Nevada Nuclear Waste Storage Investigations (NNWSI) project, administered by the Nevada Operations Office of the U. S. Department of Energy. The four units, in order of increasing stratigraphic position (decreasing depth), are as follows: 1. Tram Member of the Crater Flat Tuff, 2. Bullfrog Member of the Crater Flat Tuff, 3. The Tuffaceous beds of Calico Hills, and 4. Topopah Springs Member of the Paintbrush Tuff.

This report presents data from a series of nineteen mechanical experiments conducted on samples of Bullfrog Tuff obtained from USW-G1 core at eleven different stratigraphic levels ranging in depth from 661.4 to 804.9 m (2170. to 2641. ft). The test specimens were saturated and deformed at nominal strain rate, confining pressure and temperature conditions of 10^{-5} sec^{-1}, 0.1 MPa and 23°C, respectively.

It must be pointed out that while this report is presenting only the experimental techniques and resulting data from a series of tests on Bullfrog Tuff, a detailed analysis of the mechanical data from Yucca Mountain tuffs, in general, will be reported following structural testing of the three other targeted horizons.

EXPERIMENTAL TECHNIQUES

Test Apparatus and Techniques

The mechanical experiments were performed on a load frame having a maximum load capacity of 1.0 MN (200 kip). A constant displacement rate of the loading piston is achieved by servo-control of the hydraulic loading ram while monitoring an LVDT (linear variable displacement transformer) at the base of the loading column.

Throughout this test series, axial stresses were calculated by dividing the forces, measured on a standard load cell, by the original cross-sectional area of the sample. Axial strains were calculated by averaging the measured displacements on two diametrically opposed LVDT's mounted directly on the sample and dividing the average value by the original gage length. Lateral (transverse) displacements were measured across one sample diameter by a disk gage (as described by Schuler, 1978). Lateral strains were then obtained by dividing the displacements by the diameter of the test specimen. Volumetric strains were computed from axial and transverse strain data. Axial force, axial displacement, transverse displacement, ram displacement and time data were collected, reduced and plotted by a mini-computer, and then stored on cassette tapes.

Calibrations

The test system load cell is calibrated against a standard transducer once a year. The most recent load cell evaluation was performed July 1, 1981. The axial displacement LVDT's and transverse displacement gage were calibrated with a standard micrometer head prior to the test series. Calibration data for the load cell, LVDT's and gage are listed in Table I.

As a calibration test of the entire mechanical testing system, an aluminum sample of known mechanical properties was tested. The resultant data are listed and plotted in Table II and Figure 1, respectively.

Sample Preparation

The samples were all right circular cylinders recored from drillhole USW-G1 core material. The experimental specimens were 2.53 cm (.998 in) in diameter and ranged in lengths from 4.94 to 6.01 cm (1.95 to 2.37 in). The samples were stored in ground water from well J-13 (NTS) and, while submerged, subjected to a vacuum ($\leq$ 2 Torr = 267 Pa) for 18 hours in order to be sure of sample saturation. Each sample was placed between steel end pieces and jacketed in polyolefin shrink tubing. The disk gage and two LVDT's were then mounted on the specimen, the sample assembly placed between the loading ram and the load cell and the mechanical experiment begun.

EXPERIMENTAL RESULTS

Test Conditions

The nineteen mechanical experiments in this series are all unconfined compressive tests run at a nominal strain rate of 10^{-5} sec^{-1} and room temperature (approximately 23°C). The samples were obtained from eleven depth intervals of USW-G1 core. The test/sample identification used throughout this report consists of eight numbers and letters representing the drillhole (G1), sample depth (in feet) and two letters (SB, SD or SF) identifying individual samples from the same depth.

Test Data

Tabulated ultimate axial stress, axial strain to failure and elastic moduli values are given in Table III. The ranges of unconfined strengths, axial strains at failure, Young's moduli and Poisson's ratios are 4.63-153. MPa, .0028-.0058, 2.03-28.9 GPa and .08-.16, respectively.

The experimental axial stress-axial strain curves are presented in Figure 2. The general shapes of the stress-strain curves are similar:

an initial concave upward portion, a linear region, a slight concave downward portion and a sharp downward break. These curve characteristics reflect pore collapse and compaction, elastic deformation, material yield and macroscopic failure of the test specimen, respectively.

Only one sample was deformed at each of four depths (2232, 2312, 2367 and 2641 ft). The test results from these samples seem consistent in general behavioral trends with the bulk of the data and so are assumed to be representative of each depth. Test G12468SD is presented alone because the strain data for G12468SB was not retained.

Several of the curve sets show excellent reproducibility of results (e.g., Figures 2H, 2I, 2J), while Figures 2A and 2C illustrate the wide scatter which can occur in these results. The differences in stress-strain behavior of adjacent samples can be attributed to variability of matrix physical properties or, and probably more importantly, to the existence of a large void space or soft grain within a test specimen. While samples G12170SD and G12276SD (from Figures 2A and 2C) probably represent the actual general behavior of the competent rock at the respective depths, samples G12170SB and G12276SF apparently contained large volumes of void space and/or soft, weak grains (although none were macroscopically observed on the outer surface of the tested specimens).

Figure 2F is a good example of both reproducibility and an anomalous result. The stress-strain curves for samples G12429SB and SF are very similar, and appear to reflect the general behavior of that zone of tuff. The nature of curve G12429SD is totally different from the previous two, and is subsequently assumed to be anomalous.

If results from the three anomalous samples (i.e., G12170SB, G12276SF and G12429SD) are not included, the ranges of unconfined compressive

strengths and Young's moduli are reduced, from those quoted earlier, to 19.3-153. MPa and 5.34-28.9 GPa, respectively; while those for axial strains at failure and Poisson's ratio are unchanged.

The three parts of Figure 3 present axial strain-time, axial stress-axial strain and lateral strain-axial strain data from test G12563SB, along with calculated linear-regression fits to the data. These plots are shown to illustrate representative examples of fits for strain rate, Young's modulus and Poisson's ratio. Data from sample G12563SB are also used in Figure 4 to illustrate the prevailing axial stress-lateral strain and lateral strain-axial strain relationships, which are approximately linear prior to macroscopic sample failure.

SUMMARY

Nineteen samples of Bullfrog Tuff were saturated and deformed in compression at a nominal strain rate of 10^{-5} sec^{-1}, atmospheric pressure and room temperature. Although a few of the results were anomalous, most of the samples exhibited a similar axial stress-axial strain behavior resulting in macroscopic brittle failure. The resultant unconfined compressive strengths, axial strains to failure, Young's moduli and Poisson's ratios ranged from 4.63 to 153. MPa, .0028 to .0058, 2.03 to 28.9 GPa and .08 to .16, respectively.

REFERENCES

Lipman, P. W. and E. J. McKay (1965), Geologic Map of the Topopah Spring SW Quadrangle, Nye County, Nevada, USGS Map GQ-439.

Schuler, K. W. (1978), Lateral-Deformation Gage for Rock Mechanics Testing, Experimental Mechanics, V. 18, No. 12, p. 477-480.

Load Cell			LVDT's			Disk Gage		
F_{Actual}[a] (Lbs)	F_{Cell}[a] (Lbs)	Error (%)	d_{Actual}[b] (Milliinch)	d_{LVDT}[b] (Milliinch)	Error (%)	d_{Actual}[b] (Milliinch)	d_{Gage}[b] (Milliinch)	Error (%)
4000	4004	.10	5.000	4.976	-.48	5.000	5.050	1.0
8000	8010	.13	6.000	5.964	-.60	6.000	6.036	.60
12000	12006	.05	7.000	6.966	-.49	7.000	7.022	.31
16000	16000	0.0	8.000	7.978	-.28	8.000	8.022	.28
20000	19990	-.05	10.00	9.988	-.12	10.00	10.01	.10
			11.00	10.99	-.09	11.00	11.01	.09
			12.00	12.00	0.0	12.00	12.01	.08
			15.00	15.03	.20	15.00	15.04	.27
			16.00	16.04	.25	16.00	16.05	.31
			18.00	18.03	.17	18.00	18.08	.44
			20.00	20.03	.15	20.00	20.11	.55

[a] The F_{Actual} is the force measured by the standard load cell, while the F_{Cell} is the force measured by the system's load cell.

[b] The d_{Actual} is the displacement measured on the standard micrometer, while the d_{LVDT} and d_{Gage} are the displacements measured by the LVDT's and disk gage, respectively, used in the test series.

Table I. Load Cell, LVDT and Disk Gage Calibration Data

σ_{AX} (MPa)	ϵ_{AX} (Millistrain)	$-\epsilon_{LAT}$ (Millistrain)
0.0	0.0	0.0
7.00	.0992	.0411
14.1	.190	.0871
21.2	.294	.106
28.4	.390	.140
35.4	.503	.160
42.5	.607	.194
49.9	.690	.208
57.4	.802	.285
64.5	.903	.322
71.7	1.02	.348
78.9	1.12	.356
86.2	1.20	.397
93.7	1.30	.462
100.8	1.42	.489
108.6	1.54	.530
116.1	1.64	.554
123.8	1.71	.583

Table II. Aluminum Sample Calibration Data

Table III. Experimental Data

Sample ID	Depth m (ft)	$(\sigma_{AX})_u$ (MPa)	$(\varepsilon_{AX})_u$ (%)	E^a (GPa)	ν^a	ϕ^b (%)	$\rho_g{}^b$ (g/cm^3)
G12170SB	661.4(2170)	27.4	.44	9.39	---	28.1	2.48
G12170SD	661.4(2170)	47.1	.49	11.5	.11	28.1	2.48
G12232SB	680.3(2232)	19.3	.45	5.34	.12	38.7	2.44
G12276SD	693.7(2276)	26.7	.28	10.3	.12	34.2	2.40
G12276SF	693.7(2276)	4.63	.34	2.03	---	34.2	2.40
G12312SD	704.7(2312)	41.6	.34	15.8	.11	36.1	2.37
G12367SD	721.4(2367)	29.2	.50	8.38	.14	26.7	2.61
G12429SB	740.3(2429)	30.6	.55	8.71	.11	27.3	2.61
G12429SD	740.3(2429)	16.6	.50	3.93	.16	27.3	2.61
G12429SF	740.3(2429)	29.0	.52	8.01	.16	27.3	2.61
G12468SB	752.2(2468)	36.6	---	-----	---	28.0	2.60
G12468SD	752.2(2468)	46.3	.56	12.6	.14	28.0	2.60
G12563SB	781.2(2563)	120.	.58	21.9	.14	21.4	2.47
G12563SD	781.2(2563)	153.	.54	28.9	.14	21.4	2.47
G12585SB	787.9(2585)	71.7	.51	15.2	.08	24.4	2.39
G12585SD	787.9(2585)	83.7	.58	15.7	.12	24.4	2.39
G12608SB	794.9(2608)	71.9	.45	18.4	.14	23.5	2.47
G12608SD	794.9(2608)	73.5	.47	19.4	.13	23.5	2.47
G12641SD	804.9(2641)	50.2	.57	10.4	.14	27.9	2.49

a All E and ν values were calculated at .5 $(\sigma_{AX})_u$, except for the E value for sample G12170SB, which was calculated at .3 $(\sigma_{AX})_u$.
b Bulk property data from A. R. Lappin (personal communication).

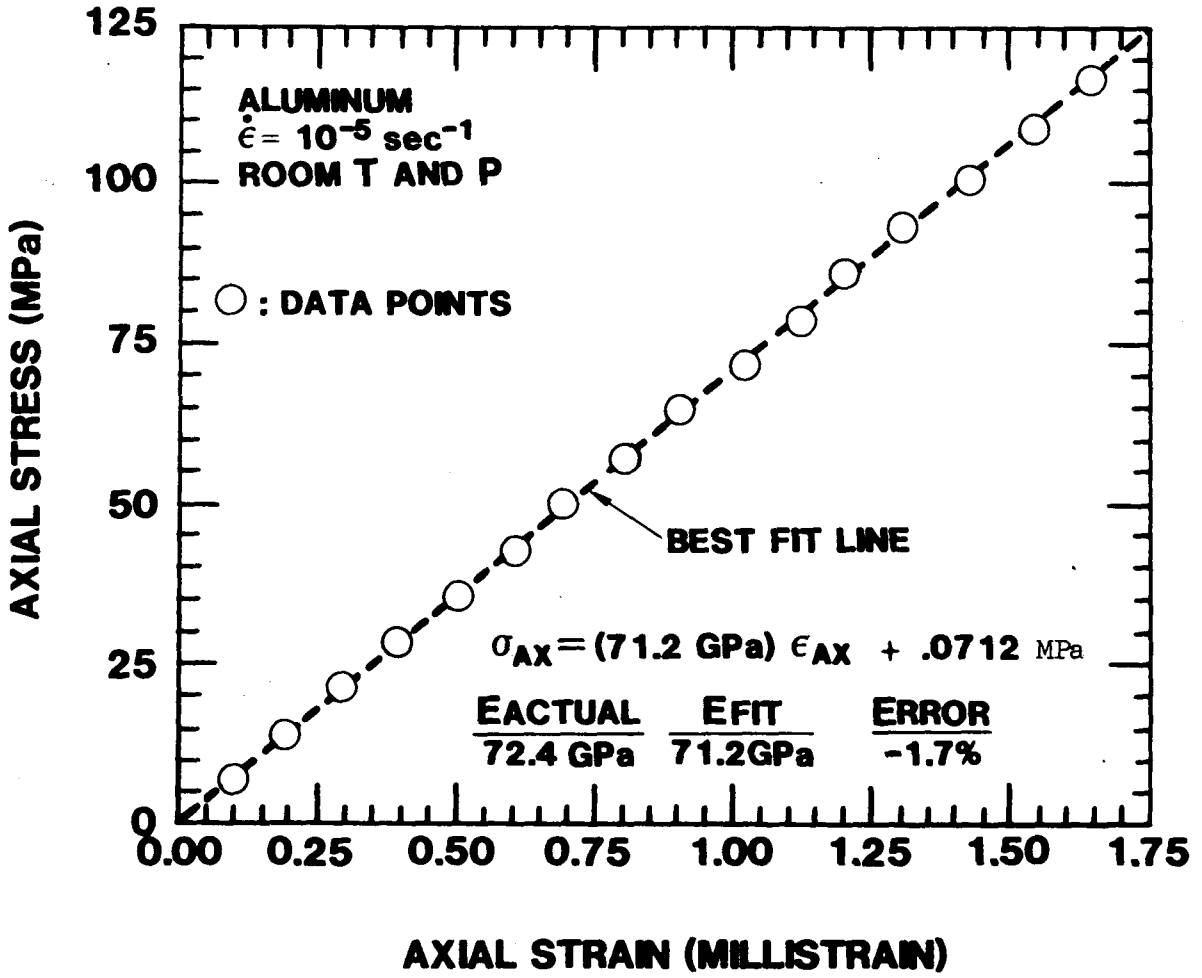

Figure 1A. Plot of axial stress-axial strain data with a linear fit for system calibration with an aluminum sample.

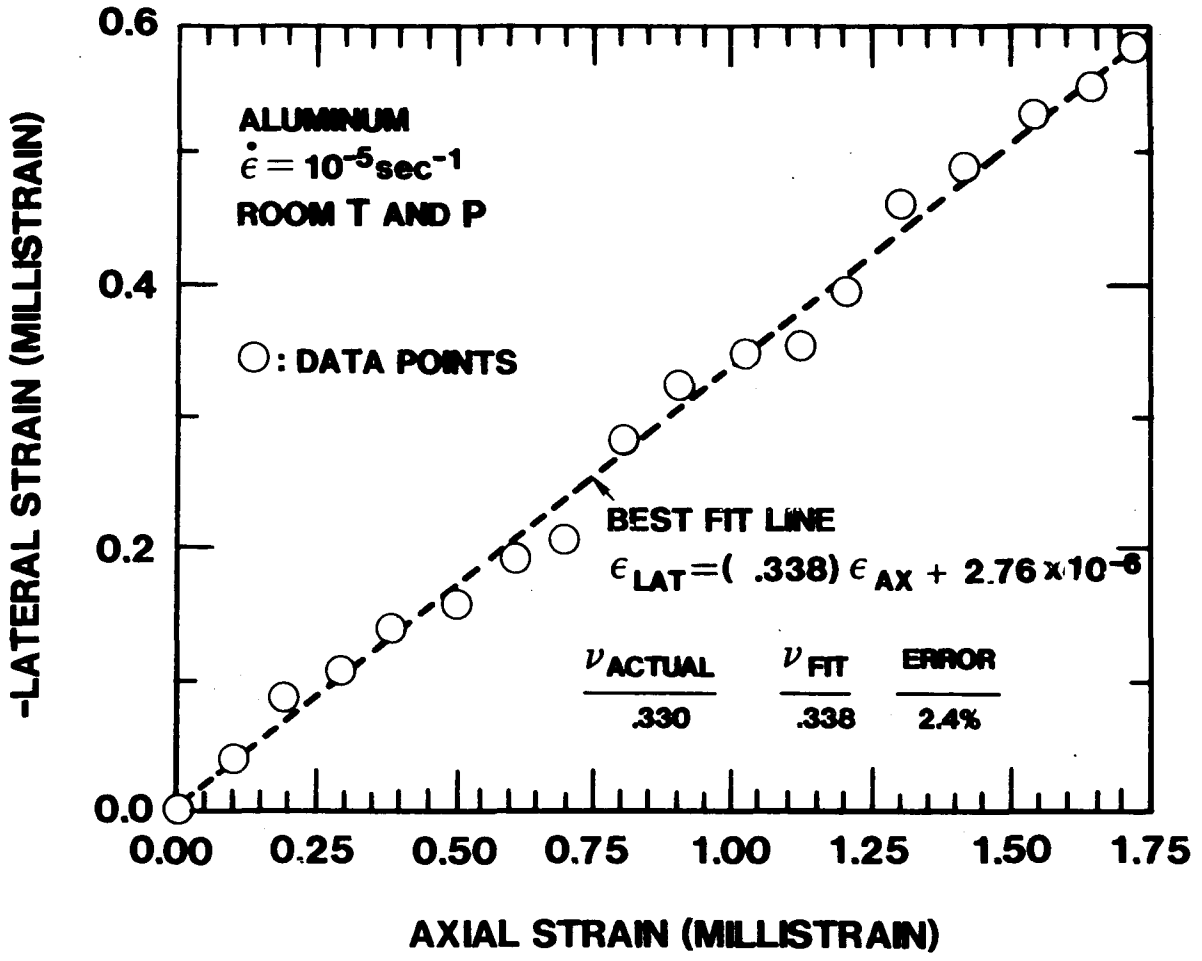

Figure 1B. Plot of lateral strain-axial strain data with a linear fit for system calibration with an aluminum sample.

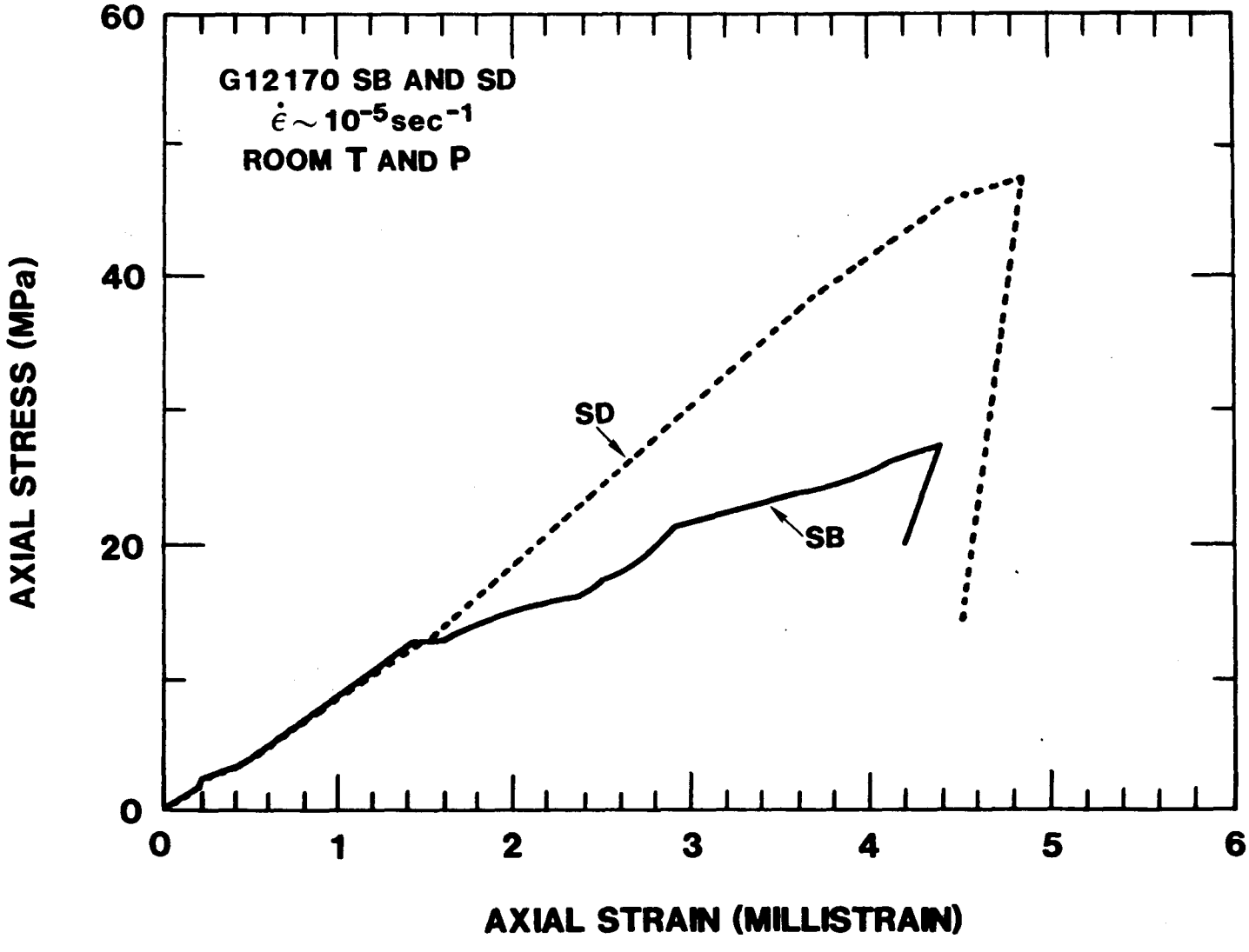

Figure 2A. Axial stress-axial strain curves for saturated samples G12170SB and SD deformed in compression at a nominal strain rate of 10^{-5} sec^{-1}, atmospheric pressure and room temperature.

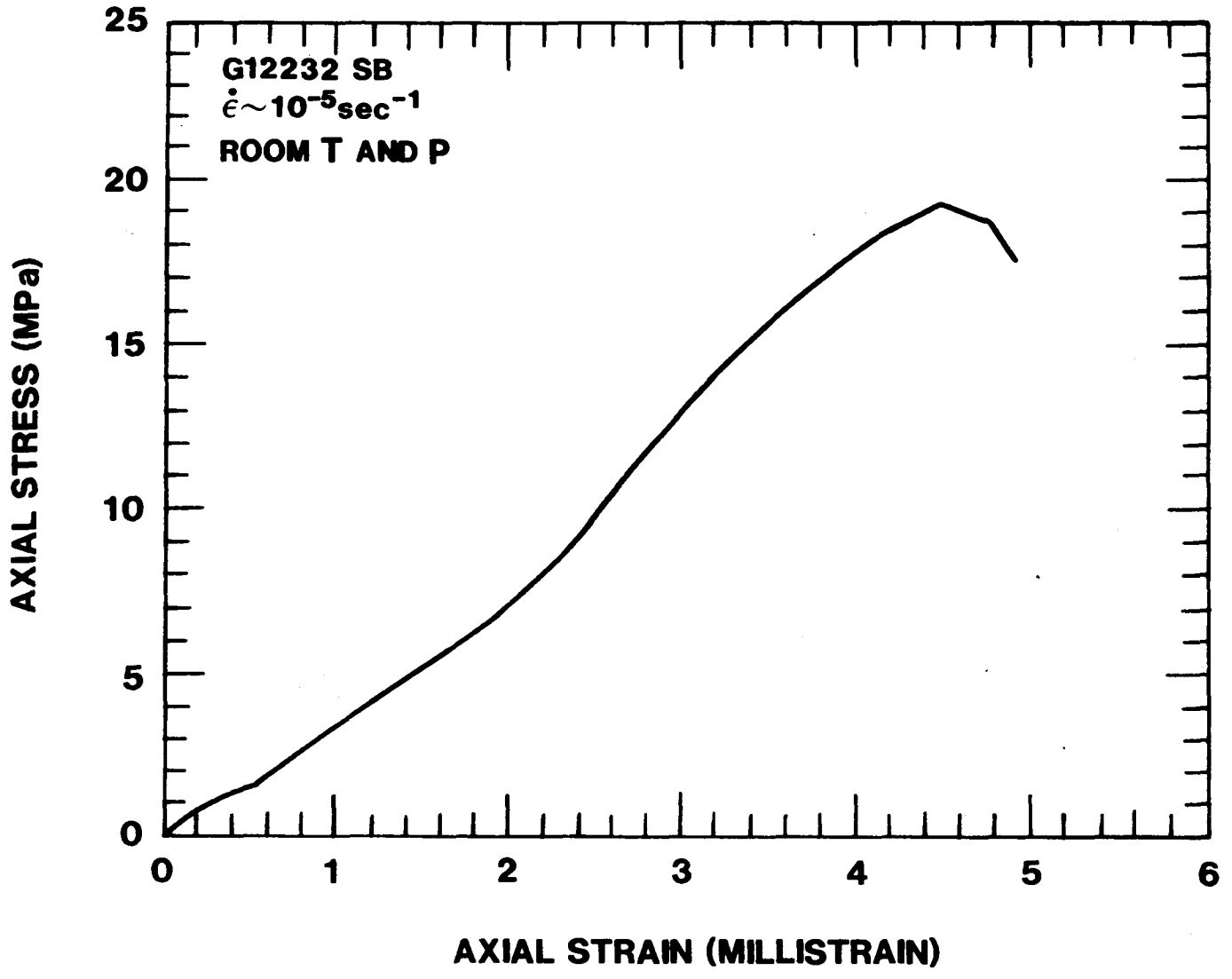

Figure 2B. Axial stress-axial strain curves for saturated sample G12232SB deformed in compression at a nominal strain rate of 10^{-5} sec^{-1}, atmospheric pressure and room temperature.

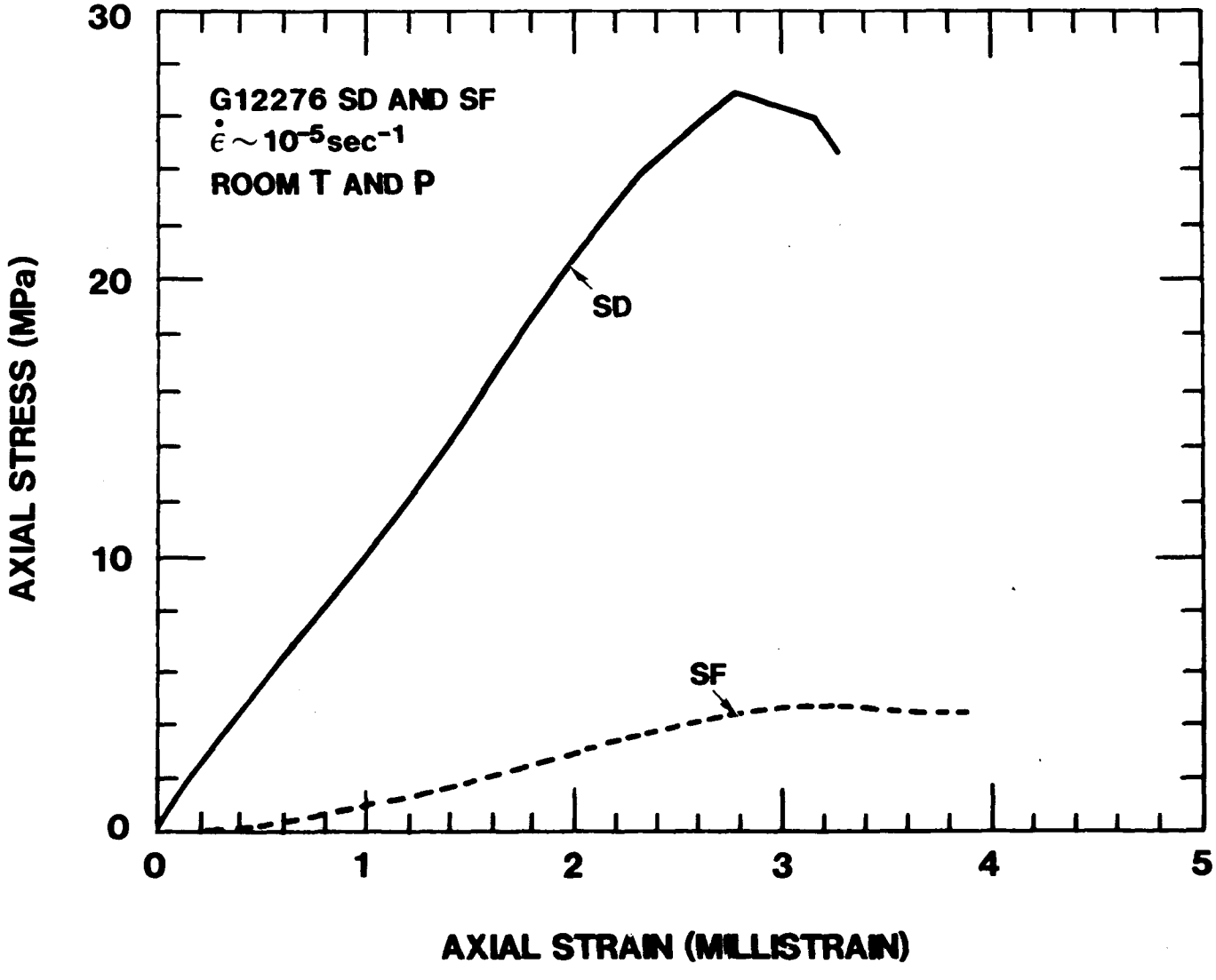

Figure 2C. Axial stress-axial strain curves for saturated samples G12276SD and SF deformed in compression at a nominal strain rate of 10^{-5} sec^{-1}, atmospheric pressure and room temperature.

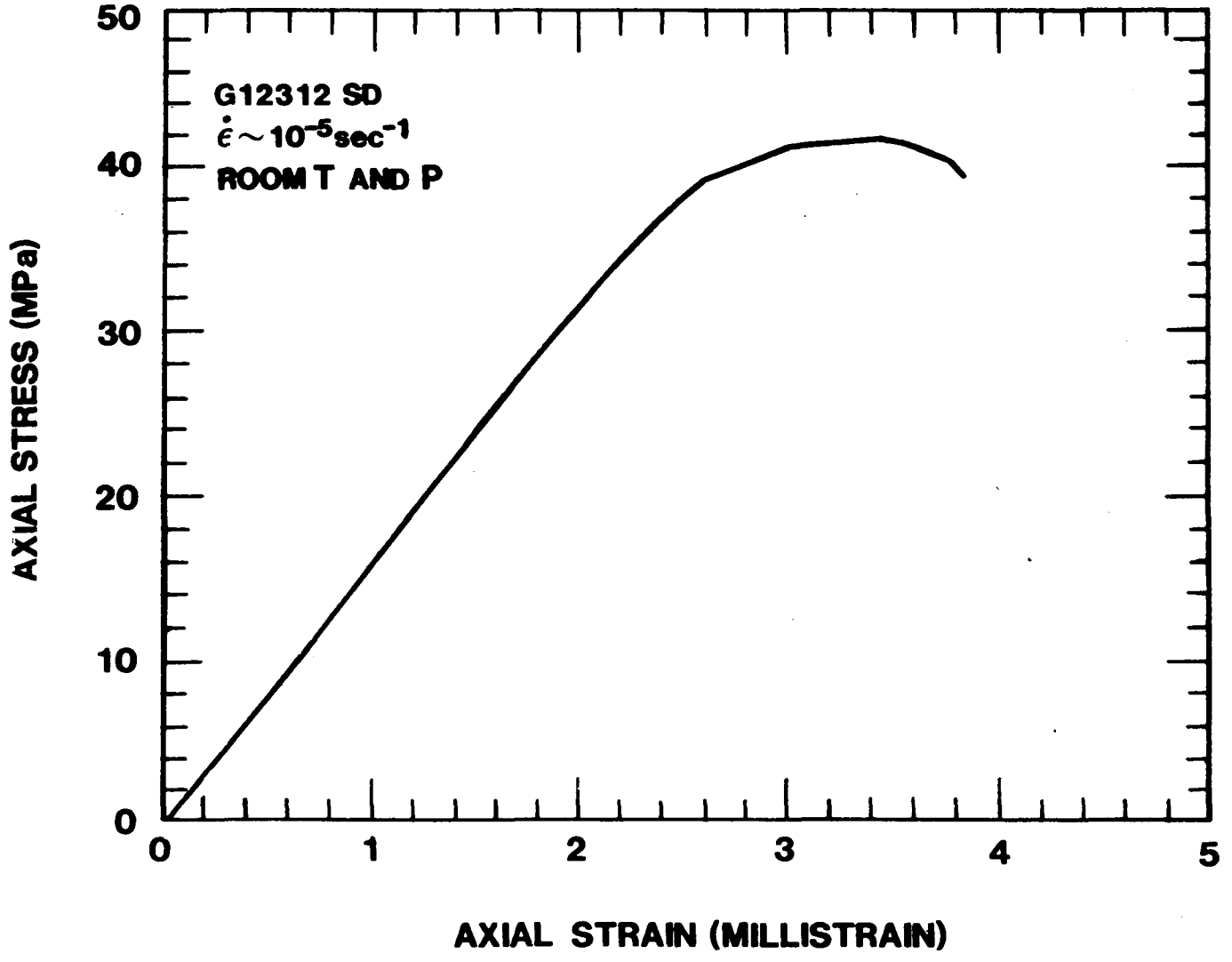

Figure 2D. Axial stress-axial strain curves for saturated sample G12312SD deformed in compression at a nominal strain rate of 10^{-5} sec^{-1}, atmospheric pressure and room temperature.

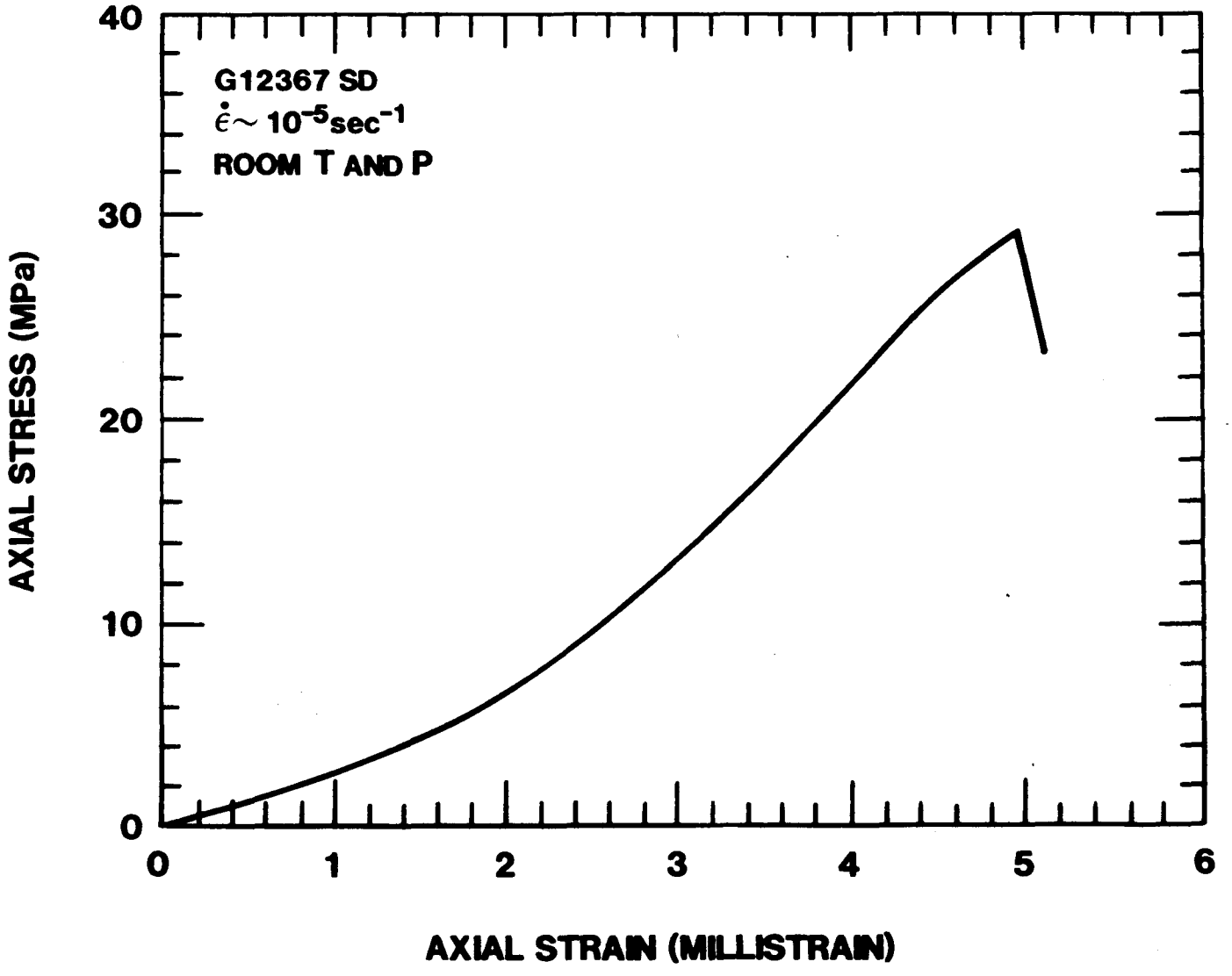

Figure 2E. Axial stress-axial strain curves for saturated sample G12367SD deformed in compression at a nominal strain rate of 10^{-5} sec^{-1}, atmospheric pressure and room temperature.

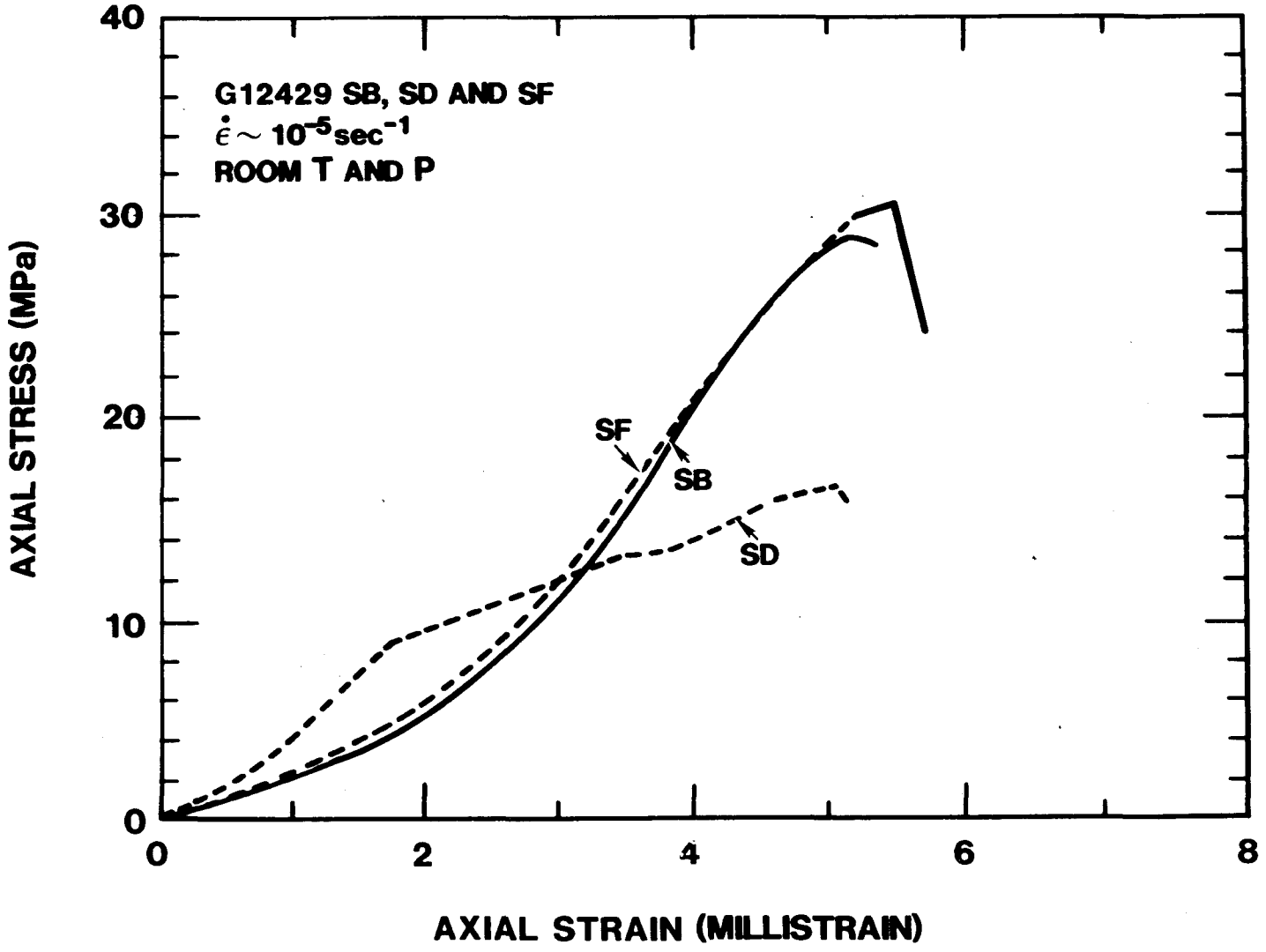

Figure 2F. Axial stress-axial strain curves for saturated samples G12429SB, SD and SF deformed in compression at a nominal strain rate of 10^{-5} sec^{-1}, atmospheric pressure and room temperature.

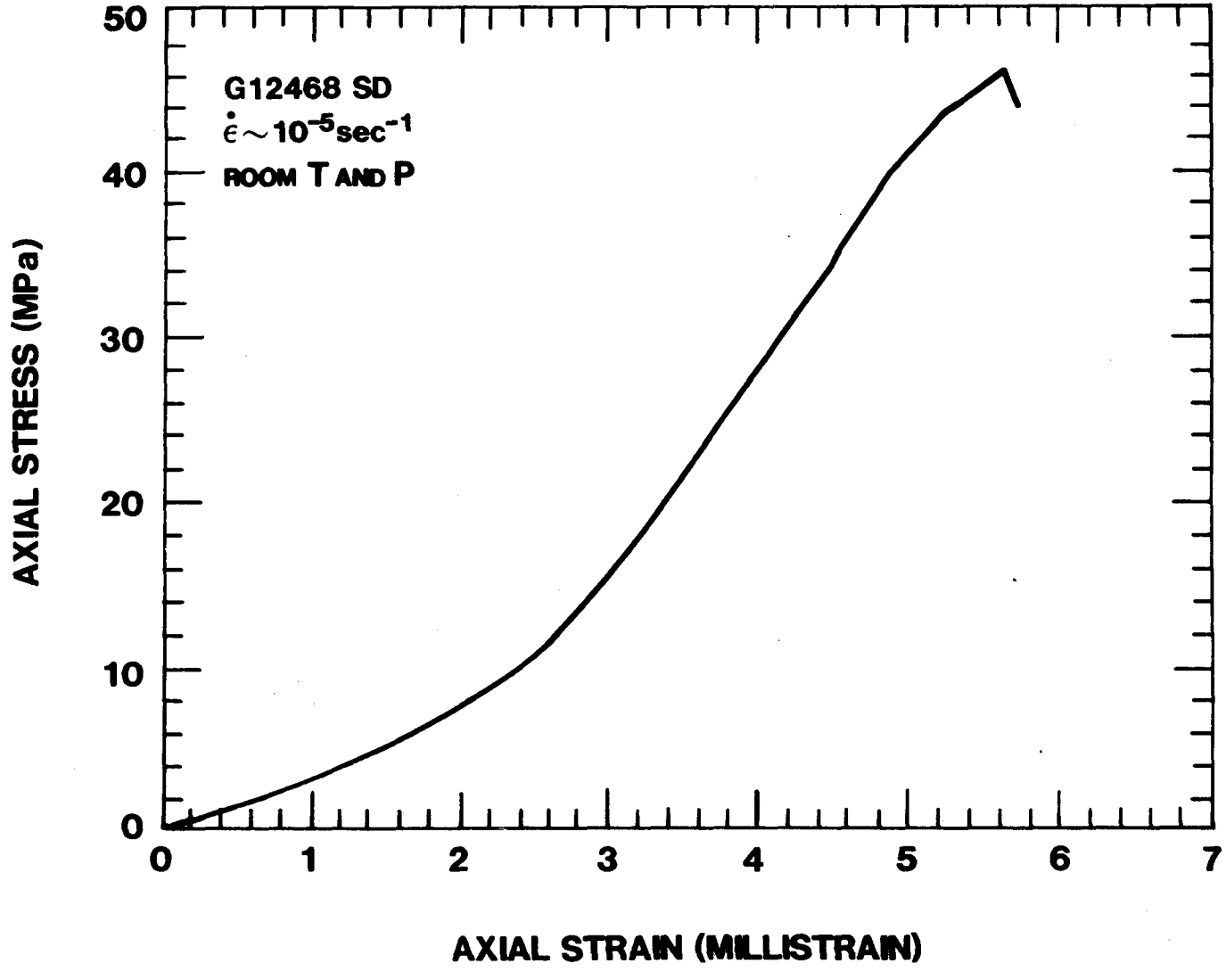

Figure 2G. Axial stress-axial strain curves for saturated sample G12468SD deformed in compression at a nominal strain rate of 10^{-5} sec^{-1}, atmospheric pressure and room temperature.

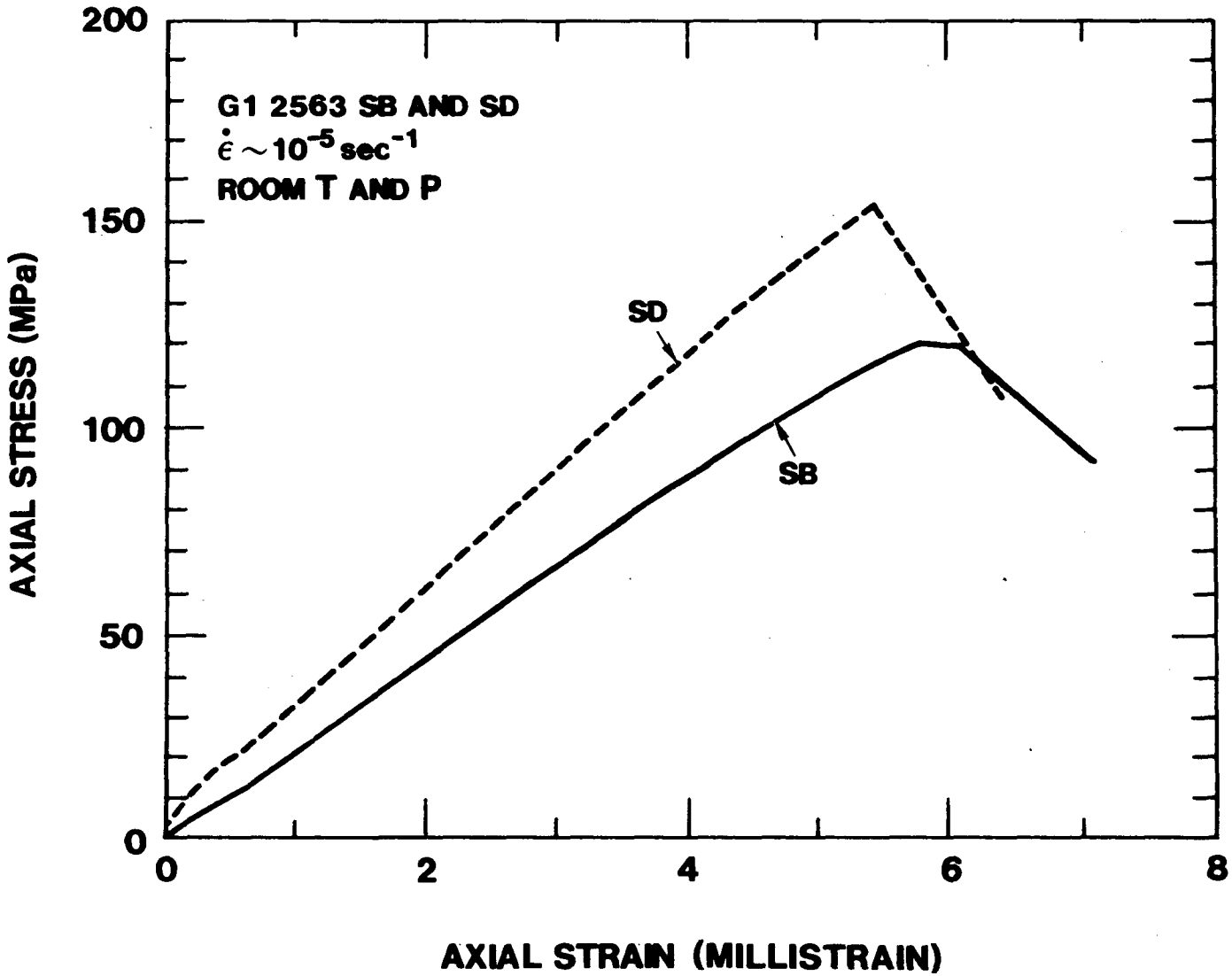

Figure 2H. Axial stress-axial strain curves for saturated samples G12563SB and SD deformed in compression at a nominal strain rate of 10^{-5} sec^{-1}, atmospheric pressure and room temperature.

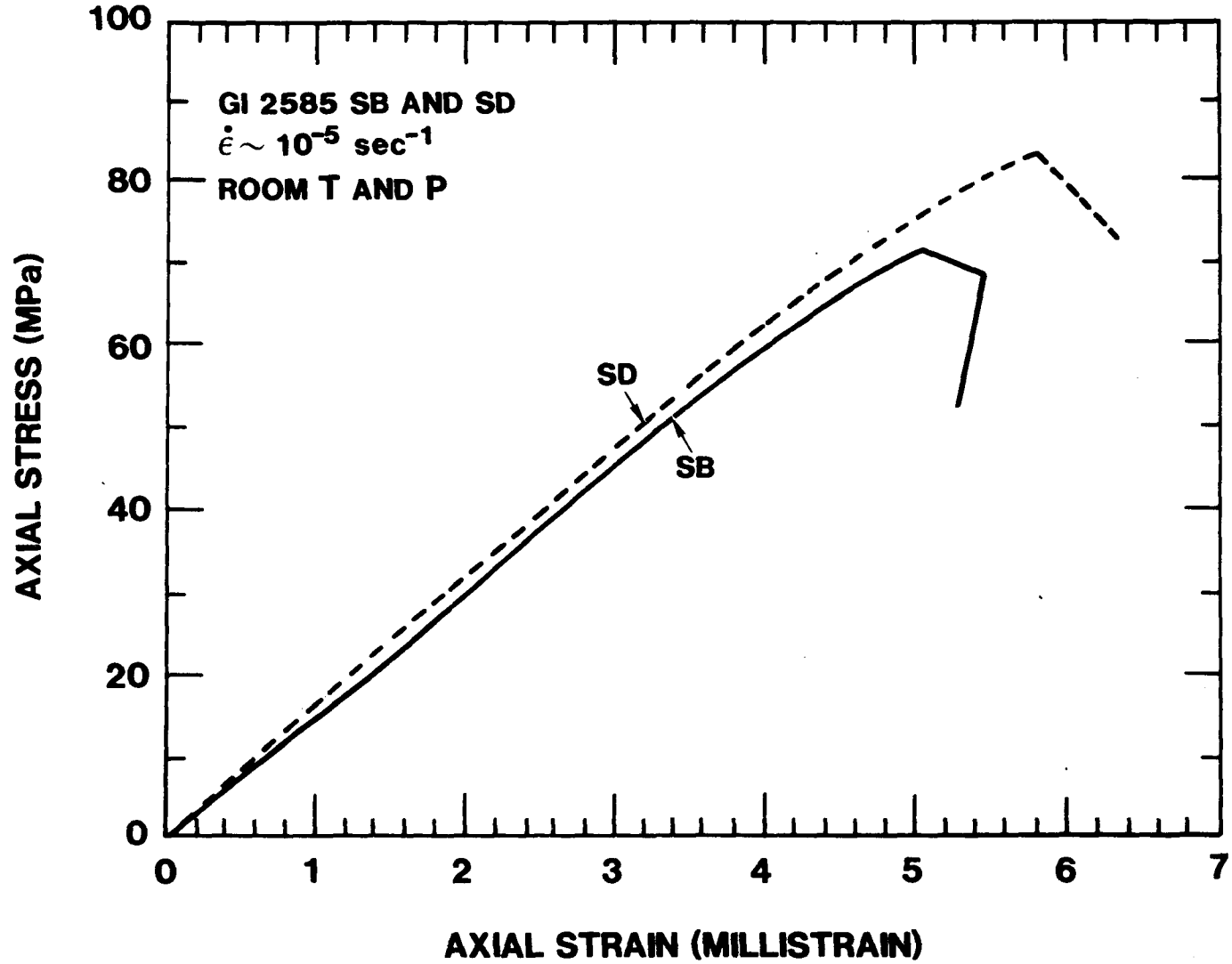

Figure 2I. Axial stress-axial strain curves for saturated samples G12585SB and SD deformed in compression at a nominal strain rate of 10^{-5} sec^{-1}, atmospheric pressure and room temperature.

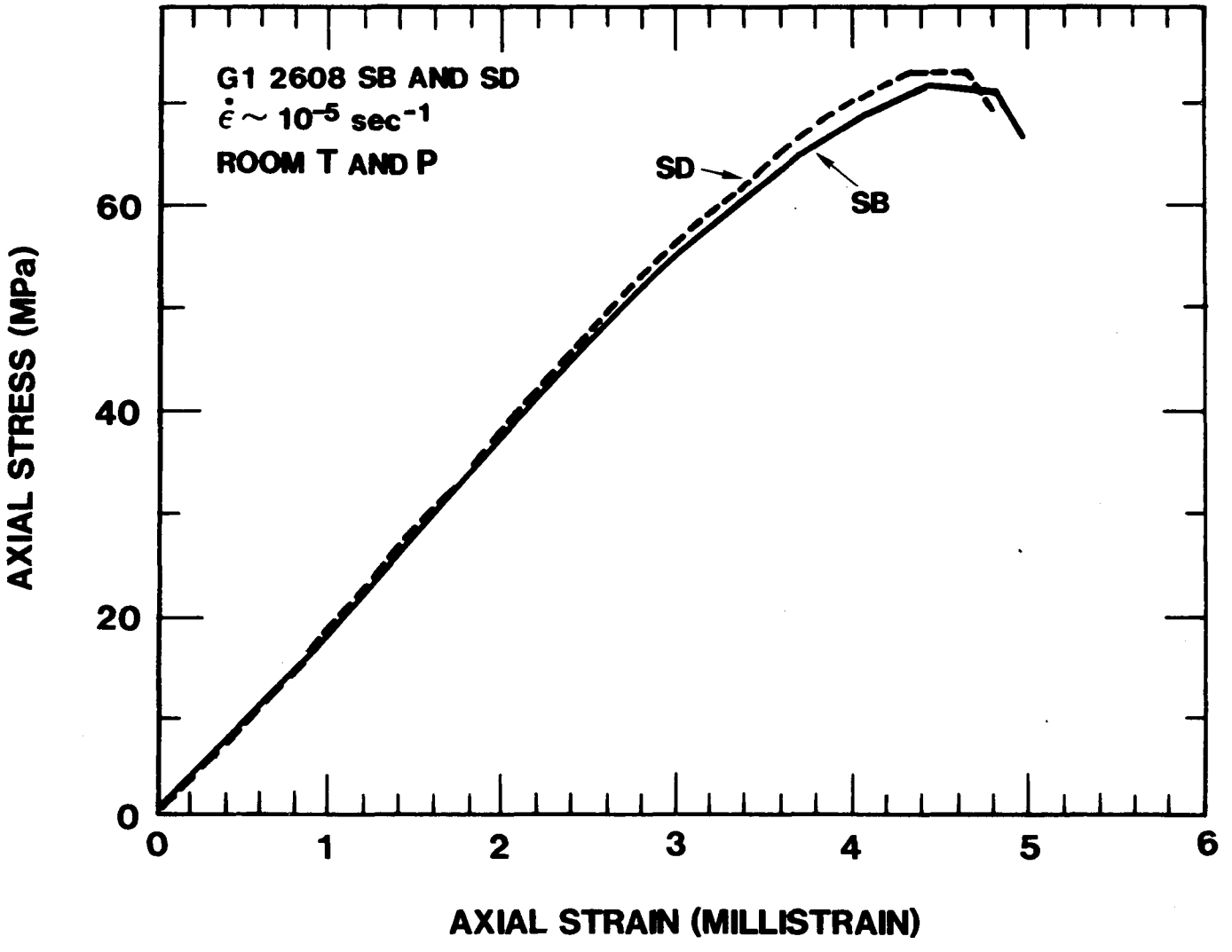

Figure 2J. Axial stress-axial strain curves for saturated samples G12608SB and SD deformed in compression at a nominal strain rate of 10^{-5} sec^{-1}, atmospheric pressure and room temperature.

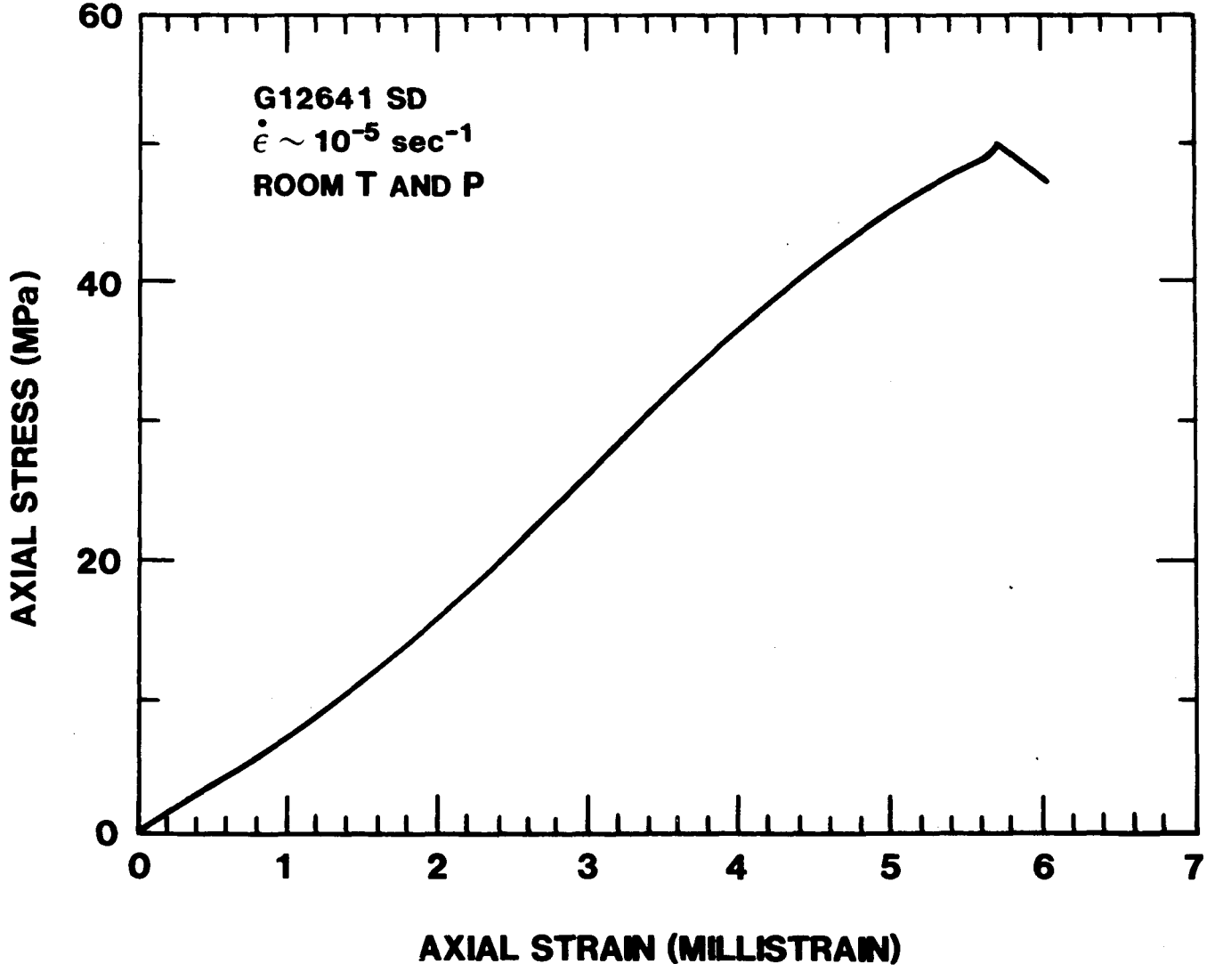

Figure 2K. Axial stress-axial strain curves for saturated sample G12641SD deformed in compression at a nominal strain rate of 10^{-5} sec^{-1}, atmospheric pressure and room temperature.

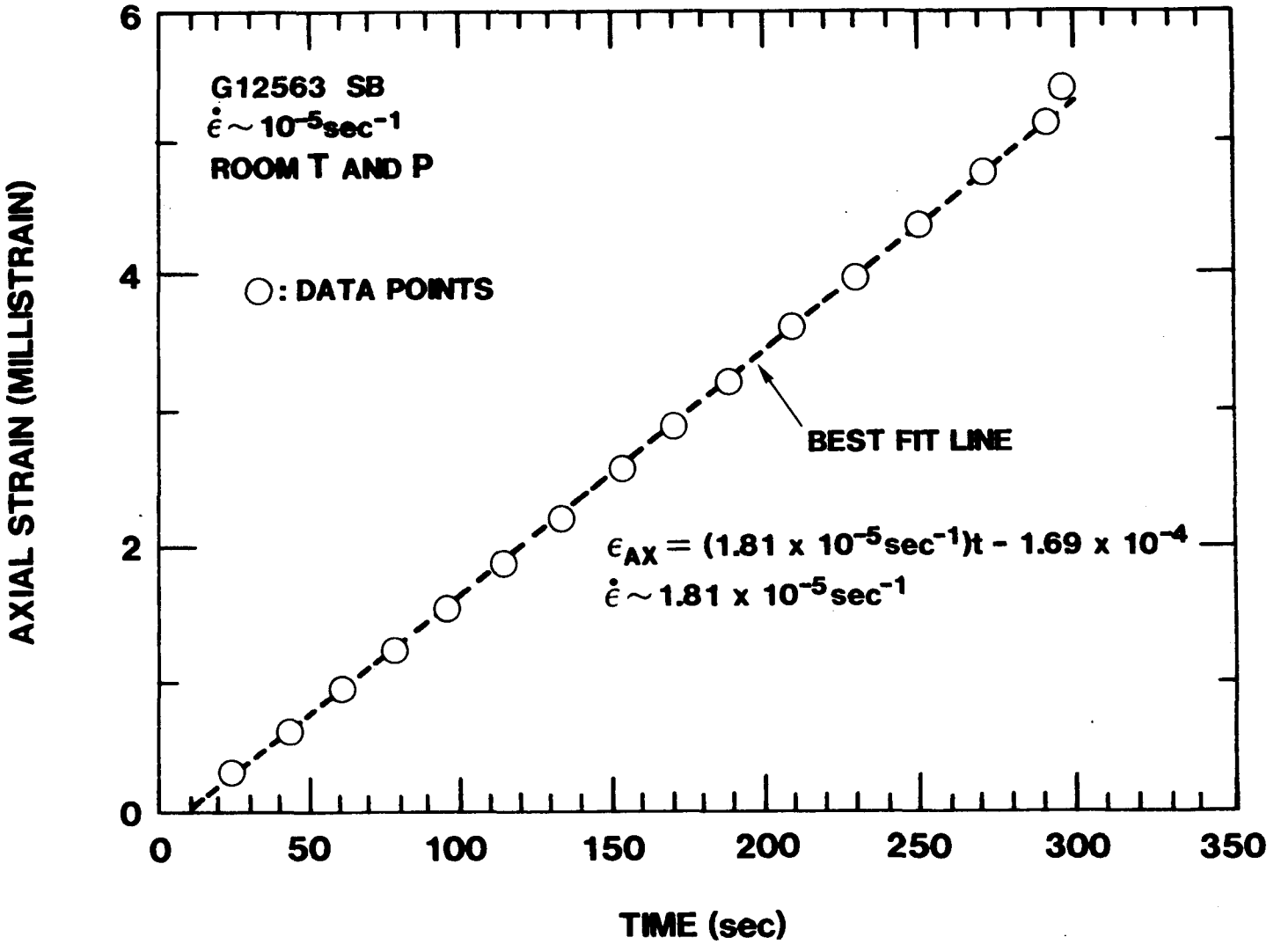

Figure 3A. Plot of axial strain-time data with a linear fit for sample G12563SB deformed saturated at 10^{-5} sec^{-1}, 0.1 MPa and 23°C.

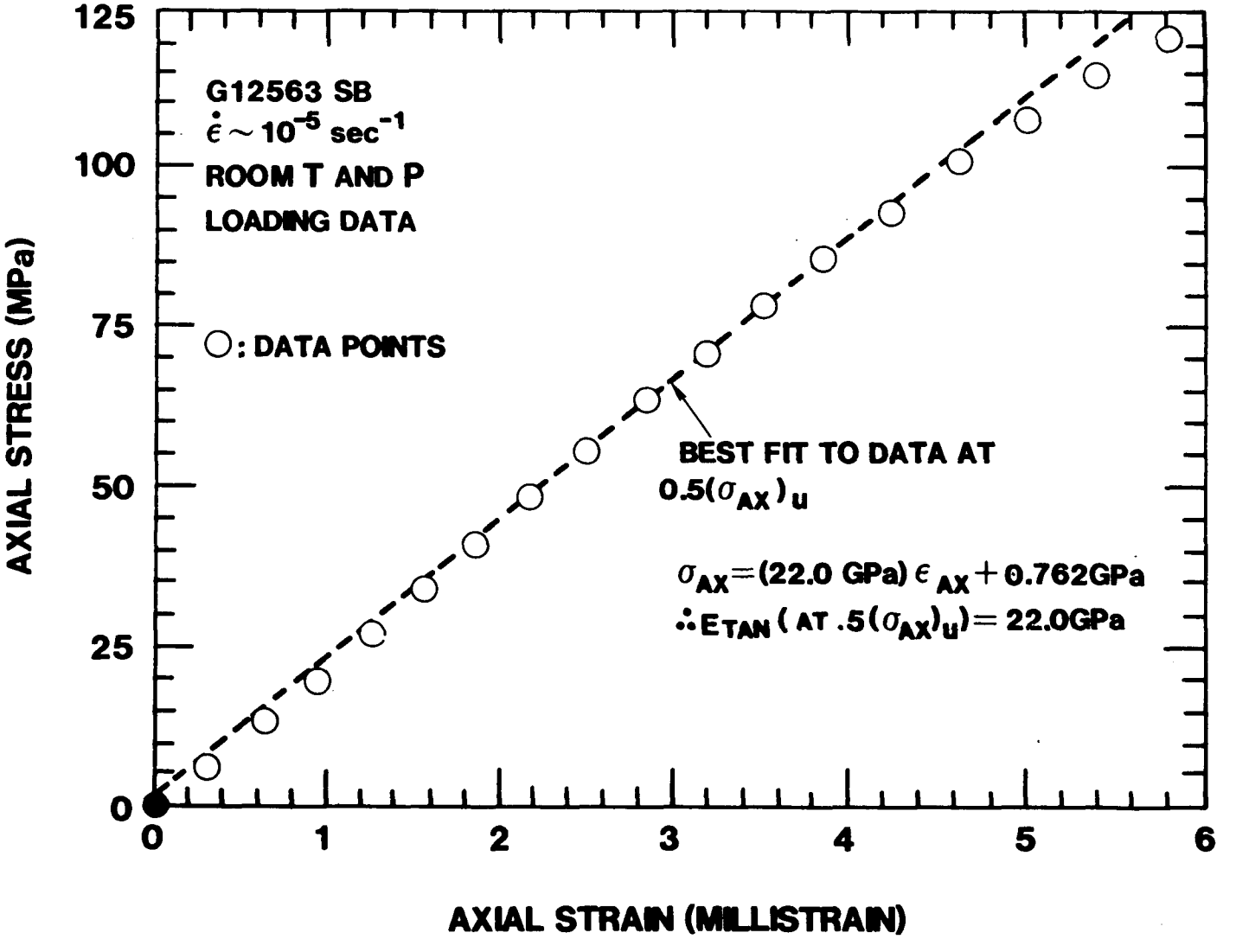

Figure 3B. Plot of axial stress-axial strain data with a linear fit for sample G12563SB deformed saturated at 10^{-5} sec^{-1}, 0.1 MPa and 23°C.

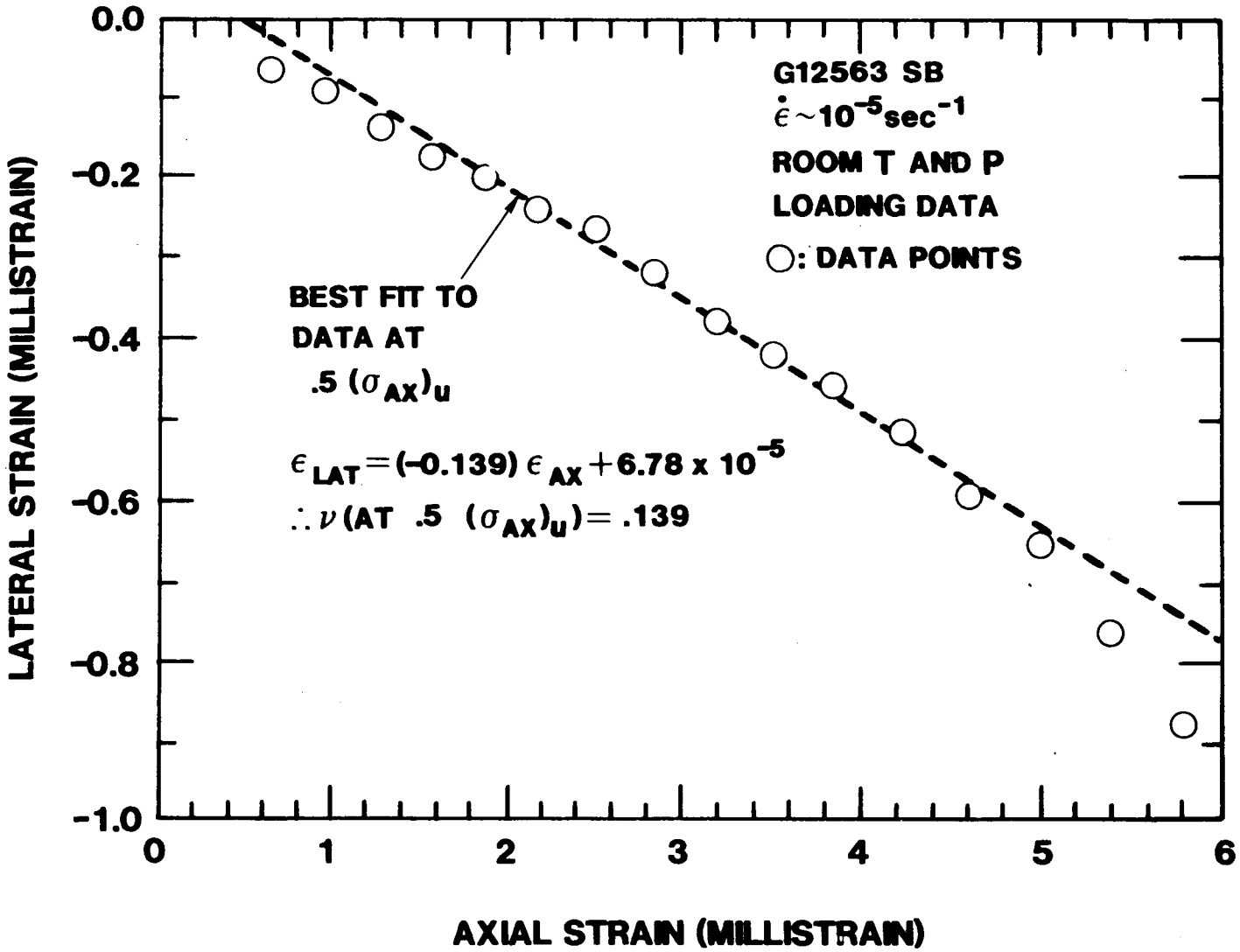

Figure 3C. Plot of lateral strain-axial strain data with a linear fit for sample G12563SB deformed saturated at 10^{-5} sec^{-1}, 0.1 MPa and 23°C.

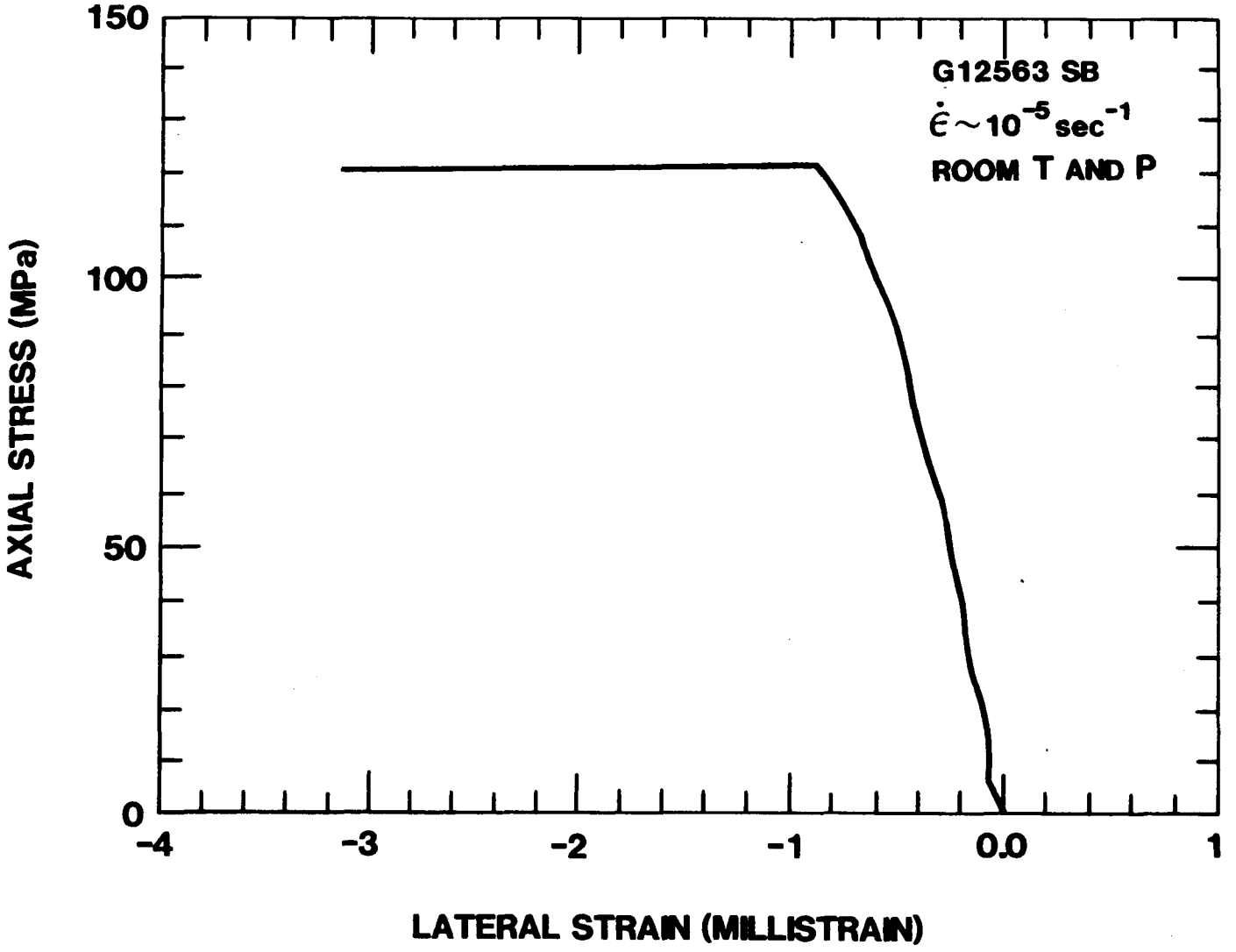

Figure 4A. Axial stress-lateral strain curve for sample G12563SB deformed saturated at 10^{-5} sec^{-1}, 0.1 MPa and 23°C.

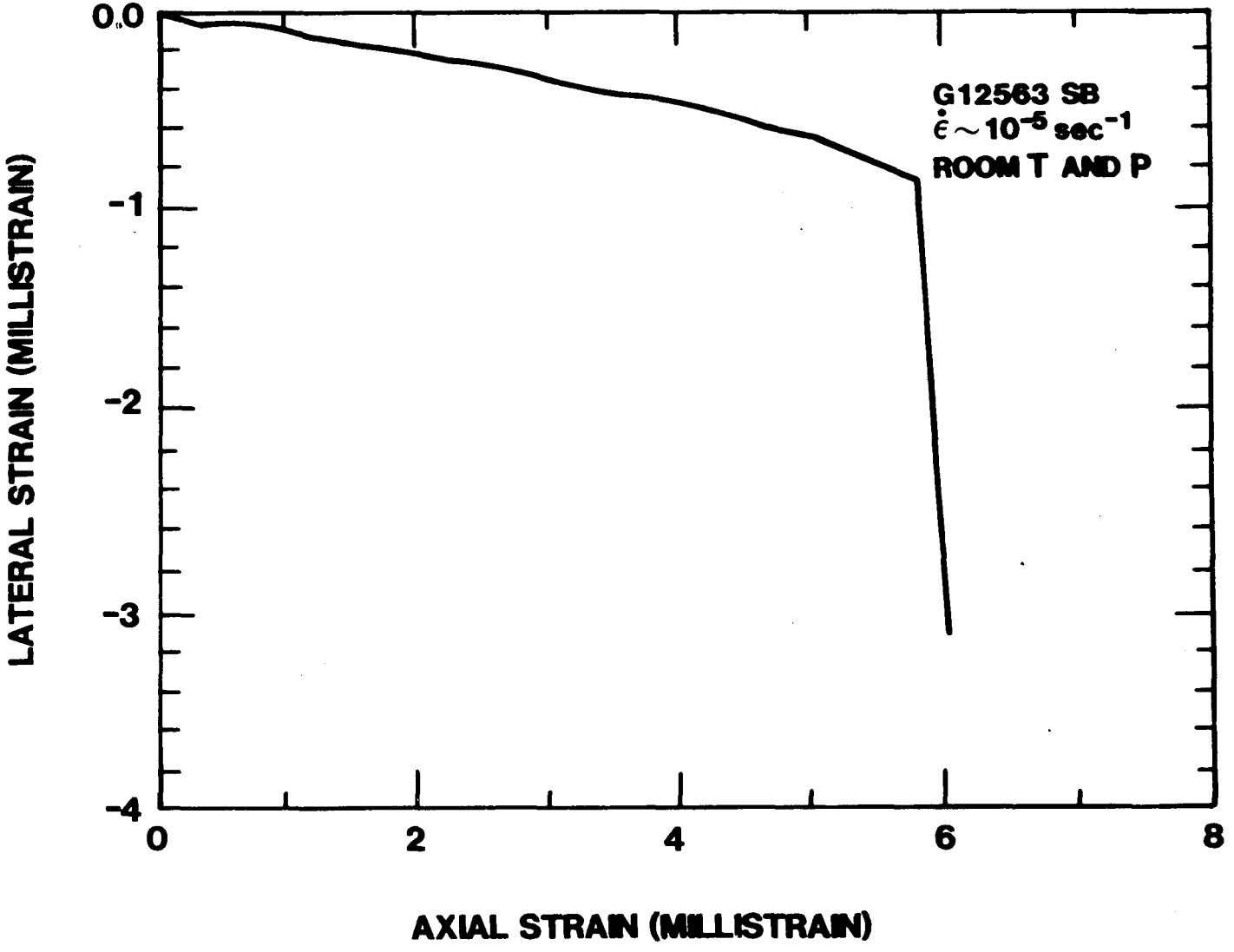

Figure 4B. Lateral strain-axial strain curve for sample G12563SB deformed saturated at 10^{-5} sec^{-1}, 0.1 MPa and 23°C.

DO NOT MICROFILM

Unlimited Release
Distribution:

C. A. Heath, Director
Office of Waste Isolation
U. S. Department of Energy
Room B-207
Germantown, MD 20767

D. L. Vieth, Acting Team Leader
Technology Team
U. S. Department of Energy
Room B-220
Germantown, MD 20767

J. O. Neff, Program Manager
National Waste Terminal
Storage Program Office
U. S. Department of Energy
505 King Avenue
Columbus, OH 43201

L. D. Ramspott
Technical Project Officer
Lawrence Livermore National
Laboratory
University of California
Post Office Box 808
Mail Stop L-204
Livermore, CA 94550

B. R. Erdal
Technical Project Officer
Los Alamos National Laboratory
University of California
Post Office Box 1663
Mail Stop 514
Los Alamos, NM 87545

R. C. Lincoln
Technical Overview Management
Sandia National Laboratories
Post Office Box 5800
Organization 4538
Albuquerque, NM 87185

A. R. Hakl, Site Manager
Westinghouse - AESD
Post Office Box 708
Mail Stop 703
Mercury, NV 89023

G. L. Dixon
Technical Project Officer
U. S. Geological Survey
Post Office Box 25046
Mail Stop 954
Federal Center
Denver, CO 80301

W. E. Wilson
U. S. Geological Survey
Post Office Box 25046
Mail Stop 954
Denver, CO 80301

A. E. Stephenson
Technical Overview Management
Sandia National Laboratories
Post Office Box 14100
Organization 4538
Las Vegas, NV 89114

L. D. Tyler
Technical Project Officer
Sandia National Laboratories
Post Office Box 5800
Organization 4532
Albuquerque, NM 87185

L. W. Scully
Technical Project Officer
Sandia National Laboratories
Post Office Box 5800
Organization 4531
Albuquerque, NM 87185

F. W. Muller
Technical Project Officer
Sandia National Laboratories
Post Office Box 5800
Organization 1417
Albuquerque, NM 87185

W. S. Twenhofel
820 Estes Street
Lakewood, CO 80226

C. R. Cooley, Deputy Director
Office of Waste Isolation
U. S. Department of Energy
Room B-214
Germantown, MD 20767

R. G. Goranson
U. S. Department of Energy
Richland Operations Office
Post Office Box 550
Richland, WA 99352

R. Deju
Rockwell International Atomics
International Division
Rockwell Hanford Operations
Richland, WA 99352

R. M. Nelson, Jr., Director (3)
Waste Management Project Office
U. S. Department of Energy
Post Office Box 14100
Las Vegas, NV 89114

D. F. Miller, Director
Office of Public Affairs
U. S. Department of Energy
Post Office Box 14100
Las Vegas, NV 89114

R. H. Marks
U. S. Department of Energy
CP-1, M/S 210
Post Office Box 14100
Las Vegas, NV 89114

B. W. Church, Director
Health Physics Division
U. S. Department of Energy
Post Office Box 14100
Las Vegas, NV 89114

R. R. Loux (7)
U. S. Department of Energy
Post Office Box 14100
Las Vegas, NV 89114

A. E. Gurrola
Holmes & Narver, Inc.
Post Office Box 14340
Las Vegas, NV 89114

K. Street, Jr.
Lawrence Livermore National
Laboratory
University of California
Mail Stop L-209
Post Office Box 808
Livermore, CA 94550

D. C. Hoffman
Los Alamos National Laboratory
Mail Stop 760
Post Office Box 1663
Los Alamos, NM 87545

R. W. Lynch
Sandia National Laboratories
Organization 4530
Post Office Box 5800
Albuquerque, NM 87185

N. E. Carter
Battelle
Office of Nuclear Waste Isolation
505 King Avenue
Columbus, OH 43201

W. A. Carbiener
Battelle
Office of NWTS Integration
505 King Avenue
Columbus, OH 43201

S. Goldsmith
Battelle
Office of Nuclear Waste Isolation
505 King Avenue
Columbus, OH 43201

ONWI Library (5)
Battelle
Office of Nuclear Waste Isolation
505 King Avenue
Columbus, OH 43201

R. M. Hill
State Planning Coordinator
Governor's Office of Planning
Coordination
State of Nevada
Capitol Complex
Carson City, NV 89023

N. A. Clark
Department of Energy
State of Nevada
Capitol Complex
Carson City, NV 89710

DO NOT MICROFILM

J. P. Colton
International Atomic Energy Agency
Division of Nuclear Power &
Reactors
Karnter Ring 11
Post Office Box 590, A-1011
Vienna, Austria

H. D. Cunningham
Reynolds Electrical & Engineering
Co., Inc.
Mail Stop 555
Post Office Box 14400
Las Vegas, NV 89114

J. A. Cross
Fenix & Scisson, Inc.
Post Office Box 15408
Las Vegas, NV 89114

A. M. Friedman
Argonne National Laboratories
9700 S. Cass Avenue
Argonne, IL 60439

David K. Parrish
RE/SPEC, Inc.
Post Office Box 725
Rapid City, SD 57701

John W. Handin
Center for Tectonophysics
Texas A&M University
College Station, TX 77843

4537 J. R. Tillerson
4537 A. R. Lappin
5500 O. E. Jones
5510 D. B. Hayes
5520 T. B. Lane
5521 R. K. Thomas
5530 W. Herrmann
5532 B. M. Butcher
5532 A. K. Jones
5532 K. G. Nimick
5532 W. A. Olsson
5532 R. H. Price (15)
5532 L. W. Teufel
5533 A. J. Chabai
5534 J. R. Asay
3141 L. J. Erickson (5)
3151 W. L. Garner (3)

3154-3 C. Dalin (25)
For: DOE/TIC
(Unlimited Release)
8214 M. A. Pound